BMC Complementary Medicine and Therapies

RESEARCH

Open Access

Boric acid and quercetin supplementations alleviated paraquat-induced neurotoxic and irritation effects in human SH-SY5Y cells and in ovo models

Adem Güner[1†] and Aşkın Tekin[2*†]

Abstract

Background Paraquat (PQ) is a herbicide that causes neurotoxicity through oxidative stress, mitochondrial dysfunction and apoptosis. Boric acid (BA) and quercetin (Qe) are bioactive compounds with antioxidant and anti-inflammatory properties, but their combined effect against PQ-induced neuronal damage is still unexplored. This study aimed to investigate the individual and synergistic protective effects of BA and Qe in SH-SY5Y neuroblastoma cells and *in ovo* models.

Methods Human SH-SY5Y neuroblastoma cells were exposed to PQ (400 µM) with or without BA (50 µM), Qe (50 µM) or their combination for 48 h. ROS production, mitochondrial membrane potential (MMP, ΔΨm) and intracellular calcium levels (Ca^{2+}) were measured. Apoptotic (BAX, BCL2, Casp-3) and inflammatory (NFKB, VEGF, TNF, TRAF1) gene expression and DNA fragmentation were determined by qRT-PCR and DPA assay. NRF2 activation was determined by gene expression. In parallel, irritation and vascularization were evaluated using the hen's egg chorioallantoic membrane (HET-CAM) assay after exposure to PQ, BA, Qe and their combinations.

Results PQ significantly increased ROS, interfered with MMP, increased Ca^{2+} levels, regulated pro-apoptotic and inflammatory genes, and induced DNA fragmentation. BA or Qe alone reduced oxidative stress, partially restored ΔΨm and Ca^{2+} homeostasis, downregulated BAX and Casp-3, and increased BCL2 expression. The combined treatment with BA + Qe showed the strongest protection by significantly reducing ROS, restoring ΔΨm and Ca^{2+} homeostasis, suppressing inflammatory genes, enhancing NRF2 activation and minimizing DNA fragmentation, indicating synergistic antioxidant and anti-apoptotic effects. In the HET-CAM assay, PQ induced hemorrhage, lysis, and severe irritation with an IS of 9.1 ± 0.2, whereas BA, Qe, and BA + Qe alone showed no irritation. Co-treatments (BA + PQ and Qe + PQ) caused moderate irritation (IS 6.2 ± 0.1 and 6.0 ± 0.2, respectively), while the combined treatment with BA + Qe + PQ markedly alleviated irritation, showing only mild effects (IS 4.1 ± 0.2).

Conclusions BA and Qe, particularly in combination, protect neuronal cells from PQ-induced oxidative and mitochondrial damage by restoring redox balance, stabilizing mitochondria, regulating Ca^{2+} homeostasis and

[†]Adem Güner and Aşkın Tekin contributed equally to this work.

*Correspondence:
Aşkın Tekin
askin.tekin@giresun.edu.tr

Full list of author information is available at the end of the article

© The Author(s) 2025. **Open Access** This article is licensed under a Creative Commons Attribution-NonCommercial-NoDerivatives 4.0 International License, which permits any non-commercial use, sharing, distribution and reproduction in any medium or format, as long as you give appropriate credit to the original author(s) and the source, provide a link to the Creative Commons licence, and indicate if you modified the licensed material. You do not have permission under this licence to share adapted material derived from this article or parts of it. The images or other third party material in this article are included in the article's Creative Commons licence, unless indicated otherwise in a credit line to the material. If material is not included in the article's Creative Commons licence and your intended use is not permitted by statutory regulation or exceeds the permitted use, you will need to obtain permission directly from the copyright holder. To view a copy of this licence, visit http://creativecommons.org/licenses/by-nc-nd/4.0/.

modulating apoptosis and attenuating irritation in the *in ovo* model. These results suggest that BA and Qe may be promising complementary therapeutics to attenuate neurotoxicity caused by environmental toxins.

Keywords Boric acid, Inflammation, Neurotoxicity, Oxidative stress, Paraquat, Quercetin

Introduction

Paraquat (1,1'-dimethyl-4,4'-bipyridylium dichloride; PQ) is widely used to control crops such as cocoa, cotton, rice, soya beans and vegetables. It is highly persistent in the environment, with less than 20% microbial degradation in river waters after 56 days and therefore poses a significant risk of long-term contamination [1, 2]. Overuse and mismanagement of pesticides have led to food contamination and environmental pollution, raising major concerns for ecosystems and human health [3, 4]. Due to its high toxicity, PQ has been banned in many countries [3, 5]. PQ exposure occurs mainly through ingestion, inhalation or skin contact, and it accumulates in multiple organs, including the brain, lungs, kidneys and liver, often leading to multi-organ failure. Importantly, the central nervous system (CNS) is a primary target of PQ toxicity, and epidemiological evidence links occupational or environmental exposure to an increased risk of Parkinson's disease [6, 7].

PQ is a potent generator of reactive oxygen species (ROS) via redox cycling at mitochondrial complex [8]. This excessive ROS production leads to oxidative stress, mitochondrial dysfunction, impaired ATP production and apoptosis in dopaminergic neurons. PQ also downregulates the Nrf2 signaling pathway, thereby weakening neuronal antioxidant defenses. In experimental models, PQ exposure results in dopaminergic neuron loss, α-synuclein aggregation, mitochondrial fission and activation of pro-inflammatory signaling such as NF-κB and the NLRP3 inflammasome [7, 9]. Furthermore, PQ increases lipid peroxidation, depletes glutathione (GSH), reduces superoxide dismutase (SOD) activity and causes genotoxic effects, including DNA strand breaks and Ca^{2+} dysregulation [6, 7, 10–12]. Collectively, these studies underline the multifaceted neurotoxic potential of PQ. Despite its high fatality rate, no effective treatments are currently available [13]. Antioxidants have a protective effect and alleviate the consequences of exposure to PQ.

Quercetin (Qe) is a natural flavonoid abundant in fruit, vegetables and tea. It exerts antioxidant, anti-inflammatory and neuroprotective effects by scavenging ROS, stabilizing mitochondria and modulating signaling pathways such as Nrf2/HO-1 and NF-κB. In PQ-induced neurotoxicity models, Qe restores GSH levels, reduces lipid peroxidation and upregulates antioxidant enzymes [14]. It also inhibits microglial activation and the release of pro-inflammatory cytokines [15]. The ability of Qe to cross the blood–brain barrier has been well studied and is considered a key factor in its neuroprotective effects [14, 16, 17].

Boric acid (BA) exerts neuroprotective effects mainly by mitigating oxidative stress, enhancing antioxidant defenses, and modulating apoptosis. In traumatic brain injury models, BA decreases lipid peroxidation (MDA) and increases catalase activity (CAT), indicating reduced oxidative damage and improved antioxidant response [18]. It also protects against fluoride-induced neurotoxicity by maintaining membrane integrity, improving SOD activity, and preserving DNA stability [19]. Furthermore, BA attenuates ER-stress-related apoptosis by downregulating caspase-*3* and ER stress markers such as GRP78 and CHOP [20]. In Alzheimer's disease models, BA improves learning and memory while reducing MDA and supporting antioxidant defenses [21]. At the molecular level, BA activates protective stress pathways including eIF2α/ATF4 and Nrf2/ARE, which enhance antioxidant capacity and prevent DNA [22]. Overall, these studies highlight BA's multi-faceted approach to neuroprotection, which includes modulation of oxidative stress, strengthening of antioxidant defenses and inhibition of apoptotic pathways. Given its low toxicity profile and its ability to synergies with other antioxidant compounds, BA is a promising candidate for complementary therapies aimed at alleviating nerve damage and promoting central nervous system health.

To the best of our knowledge, no previous study has systematically evaluated the effects of BA, either alone or in combination with Qe, on PQ-induced neurotoxicity. While both compounds have individually been studied for their antioxidant and neuroprotective properties in distinct models, their potential synergistic interaction in the context of PQ-mediated oxidative and inflammatory damage remains unexplored. This represents a critical gap because PQ remains a globally relevant environmental toxicant closely linked to oxidative stress and neurodegeneration, yet current therapeutic options are limited. Therefore, the present study provided the first evidence that BA alone, and more importantly BA in combination with Qe, can counteract PQ-induced oxidative stress, mitochondrial dysfunction, Ca^{2+} dysregulation, apoptosis and genotoxicity. By integrating both an in vitro neuronal model (SH-SY5Y cells) and an *in ovo* vascular model (HET-CAM), this research advances the field by addressing a novel therapeutic strategy with translational potential.

Materials and methods

Cell culture and viability

Human SH-SY5Y neuroblastoma cells (ATCC® CRL-2266™, Manassas, VA, USA) were maintained in Dulbecco's

Modified Eagle Medium (DMEM/F12; Gibco, USA) supplemented with 10% fetal bovine serum (FBS) and 1% penicillin–streptomycin (100 U/mL penicillin, 100 µg/mL streptomycin) and cells were grown at 37 °C in a humidified atmosphere containing 5% CO_2. For viability analysis, SH-SY5Y cells were seeded into 96-well microplates at a density of 1×10^5 cells/mL and allowed to attach for 24 h under identical culture conditions prior to treatment. Subsequently, the cells were treated with PQ (400 µM), BA (50 µM), Qe (50 µM), or their combinations and further incubated for 48 h under the same conditions. Cell viability was assessed using the MTT assay [3-(4,5-dimethyl-2-thiazolyl)-2,5-diphenyl-2 H-tetrazolium bromide] according to the manufacturer's instructions (Cayman Chemical Company, USA). After 3 h incubation with MTT, absorbance was measured at 570 nm using a microplate reader (BMG Labtech, Ortenberg, Germany). Viability was expressed as a percentage relative to the untreated control group.

After treatments for DAPI staining, SH-SY5Y cells were washed twice with phosphate-buffered saline (PBS) and fixed in 4% paraformaldehyde (PFA) for 15 min at room temperature. Following fixation, cells were permeabilized with 0.1% Triton X-100 in PBS for 5 min and subsequently incubated with 1 µg/mL 4′,6-diamidino-2-phenylindole (DAPI; Sigma-Aldrich, St. Louis, MO, USA) in the dark for 5 min. After staining, cells were washed with PBS and mounted onto glass slides. Nuclear morphology was visualized using a fluorescence microscope (TE-2000, Nikon, Tokyo, Japan). Quantification of DAPI-stained nuclei was performed using ImageJ software (Version 1.53k, National Institutes of Health, Bethesda, MD, USA). For each treatment group, five randomly selected non-overlapping fields per well were analyzed, and at least 300 nuclei were counted from three independent biological replicates $(n = 3)$. Data were expressed as the percentage of intact nuclei relative to the total nuclei.

The treatment concentration for BA (CAS No. 10043-35-3, Sigma-Aldrich®, St. Louis, MO, USA) was set at 50 µM based on previous studies in which this dose was shown to be non-toxic and biologically active in vitro [23]. To determine the appropriate PQ concentration, SH-SY5 cells were exposed to a range of PQ concentrations (5-1000 µM) for 48 h. Cell viability was analyzed and a concentration-dependent decrease in viability was observed. Based on the results and relevant literature, 400 µM PQ reduced cell viability by approximately 50% and this concentration was used for subsequent experiments [24, 25]. Similarly, Qe (CAS No. 849061-97-8, Sigma-Aldrich®, St. Louis, MO, USA) was tested at concentrations of 0.5, 5, 10, 50 and 100 µM. No cytotoxic effect was observed at concentrations of up to 50 µM, which is why this dose was chosen as the non-toxic effective dose for further studies [26, 27]. Each treatment group was tested in three independent biological replicates, with technical triplicates $(n = 3)$ within each test.

Lactate dehydrogenase (LDH) release assay

LDH release was assessed using a previously described method [23]. SH-SY5Y cells were seeded at 1×10^5 cells/well in 96-well plates and treated with PQ (400 µM), BA (50 µM), Qe (50 µM), or their combinations for 48 h. After incubation, LDH release was quantified using a commercial kit (E-BC-K046-S, Elabscience) according to the manufacturer's protocol, and absorbance was measured at 490 nm. LDH release was expressed as a percentage of total LDH (cells lysed with 2% Triton-X100). Untreated cells served as a negative control, while H_2O_2 (2.5×10^{-5} M, 48 h) was used as a positive control. All assays were performed in triplicate biological repeats $(n = 3)$.

Total antioxidant capacity (TAC) and total oxidative stress (TOS) activity

Total antioxidant capacity (TAC) and total oxidant status (TOS) were determined using commercial kits (E-BC-K801-M and E-BC-K802-M, Elabscience) following the protocols established in our previous work [23]. SH-SY5Y cells were seeded at 2×10^6 cells/well in 6-well plates and treated with PQ (400 µM), BA (50 µM), Qe (50 µM), and their combinations for 48 h. After incubation, culture media were collected and used for analysis.

For TAC assay, results were calibrated against Trolox and expressed as mM Trolox equivalents/L. Ascorbic acid (10^{-5} M) served as a positive control. For TOS, results were calibrated against H_2O_2 (2.5×10^{-5} M, 48 h) and expressed as µM H_2O_2 equivalents/L. All assays were performed in triplicate biological repeats $(n = 3)$.

Measurement of ΔΨm

ΔΨm was determined using a Safranin O assay by quenching, as previously described with modifications [28]. SH-SY5Y cells were seeded in 6-well plates at 2×10^6 cells/well and treated with PQ (400 µM), BA (50 µM), Qe (50 µM), or their combinations for 48 h. After treatment, cells were collected, washed with PBS and mitochondria were isolated using the Mitochondrial Isolation Kit (MITOISO1, Sigma-Aldrich) according to the manufacturer's instructions. For fluorescence measurement, 25 µg mitochondrial protein was mixed with 0.04 mM Safranin O in 100 µL. Fluorescence (Ex/Em: 495/586 nm) was measured at 37 °C using a BioTek Synergy H1 reader (Agilent Technologies, USA). The fluorescence intensity was recorded and normalized to the control group. Since Safranin O functions in quenching mode, an increase in fluorescence indicates a loss of ΔΨm (mitochondrial depolarization), whereas a decrease in fluorescence reflects preservation of ΔΨm (mitochondrial integrity). Results were expressed as % relative to the untreated control. Carbonyl cyanide 3-chlorophenylhydrazone (CCCP)(C2759, Sigma-Aldrich) was used as positive control (10 µM). All assays were performed in triplicate biological repeats $(n = 3)$.

Intracellular Ca^{2+} measurement

Intracellular Ca^{2+} measurement was performed according to the method modified by Güner and İlhan [29]. SH-SY5Y cells were seeded at a density of 1×10^6 cells/well in 6-well culture plates and allowed to adhere for 24 h at 37 °C in a humidified 5% CO_2 incubator. Cells were treated with PQ (400 µM), BA (50 µM), Qe (50 µM) and their combinations. After treatment, cells were washed twice with cold PBS to remove extracellular Ca^{2+}. The cells were then collected and resuspended in 3 mL of high purity nitric acid (65%, trace metal grade) and digested at 95 °C on a heating block until the solution became clear and colorless. After cooling, the samples were diluted in 0.2% nitric acid and filtered with a 0.22 µm membrane filter. Intracellular Ca^{2+} concentrations were determined by inductively coupled plasma–optical emission spectrometry (ICP-OES) (Thermo Scientific iCAP™ Series). Calibration curves were prepared from Ca^{2+} standard solutions (traceable to NIST, prepared in 0.2% nitric acid) in the range of 1–100 ng/mL, yielding excellent linearity (R^2 = 0.996) and a working range of 1–250 ng/10^6 cells. The limit of detection (LOD) and limit of quantification (LOQ) were 0.9 ng/10^6 cells and 1.8 ng/10^6 cells, respectively, calculated from the standard deviation of the blank and the slope of the calibration curve. Intracellular Ca^{2+} values were normalized to cell number and expressed as ng/10^6 cells. All measurements were performed in triplicate $(n = 3)$. Untreated cells were used as baseline control.

Glutathione peroxidase (GPx) activity assay

GPx activity was determined using a method previously described in our earlier study [28]. Cells were seeded at 1×10^6 cells/well in 6-well plates and treated with PQ (400 µM), BA (50 µM), Qe (50 µM), or combinations for 48 h. GPx activity was measured using the Glutathione Peroxidase Assay Kit (E-BC-K809-M, Elabscience) at 340 nm according to the manufacturer's protocol. Enzyme activity was calculated from the rate of NADPH consumption and expressed as mU/mg protein. The analysis was performed on three independent biological replicates $(n = 3)$.

Malondialdehyde (MDA) activity assay

Malondialdehyde (MDA) content was measured according to the protocol established in our previous work [28] Cells were seeded at 1×10^6 cells/well in 6-well plates and treated with PQ (400 µM), BA (50 µM), Qe (50 µM), or combinations for 48 h. MDA levels were quantified as thiobarbituric acid (TBA)-reactive substances (ab118970, Abcam, UK) at 532 nm using a Victor™ X3 multilabel reader (Perkin Elmer). Calibration curves were prepared using 1,1,3,3-tetraethoxypropane (TEP) standards within a concentration range of 0.1–10 nmol/mL. The standard curve showed excellent linearity (R^2 = 0.998). The limit of detection (LOD) and limit of quantification (LOQ), calculated from the standard deviation of the blank and the slope of the calibration curve, were 0.2 nmol/mL and 0.6 nmol/mL, respectively. MDA concentrations in the samples were interpolated from the calibration curve and expressed as nmol/mg protein. The analysis was performed on three independent biological replicates $(n = 3)$.

Superoxide dismutase (SOD) activity assay

Superoxide dismutase (SOD) activity was measured according to the protocol established in our previous work [28]. Cells were seeded at 1×10^6 cells/well in 6-well plates and treated with PQ (400 µM), BA (50 µM), Qe (50 µM), or their combinations for 48 h. SOD activity was measured using a WST-based kit (E-BC-K020-M, Elabscience) following the manufacturer's instructions. Absorbance was recorded at 450 nm, and SOD activity was calculated according to the kit formula and expressed as U/mg protein. The analysis was performed on three independent biological replicates $(n = 3)$.

Quantitative real-time polymerase chain reaction (qRT-PCR)

The effect of different concentrations of BA, Qe, PQ and their combinations on the expression levels of genes related to inflammation (TNF, IL-1β, NFKB1, TRAF1), apoptosis (BAX, BCL2, CASP3, TP53), angiogenesis (VEGF, MMP9) and oxidative stress (NRF2) was determined by qRT-PCR analysis. In brief, SH-SY5Y cells were seeded at 2×10^6 cells/well in 6-well plates and treated with PQ (400 µM), BA (50 µM), Qe (50 µM), or their combinations for 48 h. RNA was isolated using NucleoZOL (740404.200, MN). The quality of the isolated RNA was checked using NanoDrop (ND-2000c, Thermo Scientific). A first strand of cDNA was synthesized from total RNA using OneScript Plus cDNA synthesis kit (G236, ABM). Real-time polymerase chain reaction (qRT-PCR) analysis was performed using LightCycler v.1.5 (Roche Applied Science) and SYBR Green PCR Master Mix (Qiagen). The qRT-PCR reaction was performed in a 10 µL mixture containing 5 µL SYBR Green PCR Master Mix, 0.5 µL cDNA and 0.3 µM primer. The cycling conditions for the PCR reaction were as follows: initially 10 min at 95 °C, followed by 40 cycles of cyclic denaturation at 95 °C for 15 s, annealing at 59 °C for 1 min and extension for 13 s at 72 °C. The β-actin was used as an internal control. The comparative threshold cycle (Ct) method ($2^{-\Delta\Delta Ct}$ method) was used to determine the expression level of the analyzed genes. Ct values were determined for all genes at the same fluorescence threshold line, and Ct values for each sample were obtained by calculating the arithmetic mean of triplicate values. PCR was performed with specific primers for the genes listed below:

Gene	Accession Number	Primers
BAX	NM_138764	F- GAGTGTCTCAAGCGCATCG
		R- GCAAAGTAGAAAAGGGCGACA
TNF	NM_000594	F-CTCTTCTGCCTGCTGCACTTTG
		R-ATGGGCTACAGGCTTGTCACTC
Bcl2	NM_000633	F- GTGGCCTTCTTTGAGTTCGG
		R- GGCCGTACAGTTCCACAAA
Caspase-3	NM_004346	F- AGCGAATCAATGGACTCTGGA
		R- GGTTTGCTGCATCGACATCT
MMP9	NM_004994	F- TTCCAAACCTTTGAGGGCGA
		R- CAAAGGCGTCGTCAATCACC
TP53	NM_000546	F- GTCCAGATGAAGCTCCCAGA
		R- CAAGAAGCCCAGACGGAAAC
NFkB1	NM_003998	F-GCAGCACTACTTCTTGACCACC
		R-TCTGCTCCTGAGCATTGACGTC
NRF2	NM_006164	F-CACATCCAGTCAGAAACCAGTGG
		R- GGAATGTCTGCGCCAAAAGCTG
IL-1β	NM_000576	F- CCACAGACCTTCCAGGAGAATG
		R- GTGCAGTTCAGTGATCGTACAGG
VEGF	NM_001025366	F-TTGCCTTGCTGCTCTACCTCCA
		R-GATGGCAGTAGCTGCGCTGATA
TRAF 1	NM_005658	F- CGATGGCACTTTCCTGTGGAAG
		R- TACAGCCGCAGGCACAACTTGT
β-actin	NM_001101	F- CTCCATCCTGGCCTCGCTGT
		R- GCTGTCACCTTCACCGTTCC

Quantitative DNA fragmentation (DPA assay)

DNA fragmentation was quantified using the Diphenylamine (DPA) colorimetric assay, based on the protocol of Burton [30] with minor modifications. In brief, SH-SY5Y cells (1 × 10⁵6 cells/well) were seeded in 6-well plates and treated with PQ (400 µM), BA (50 µM), Qe (50 µM), or combinations for 48 h. After treatment, cells were harvested and lysed in hypotonic lysis buffer (10 mM Tris-HCl, 10 mM EDTA, 0.5% Triton X-100, pH 7.4), followed by centrifugation at 13,000 × g for 20 min at 4 °C to separate fragmented DNA (supernatant) from intact chromatin (pellet). Both fractions were precipitated overnight at 4 °C with 12.5% trichloroacetic acid (TCA) and then hydrolyzed in 5% TCA at 90 °C for 15-minutes. After cooling, 1 mL of freshly prepared (DPA) reagent (150 mg DPA in 10 mL glacial acetic acid with 150 µL concentrated sulphuric acid and 50 µL 1.6% acetaldehyde solution) was added to each tube. The samples were incubated at 37 °C for 4 h and the color intensity was measured spectrophotometrically at 600 nm. All assays were performed in triplicate biological repeats $(n = 3)$. Results expressed as % fragmented DNA relative to total DNA.

The percentage of fragmented DNA was calculated using the formula:

$$\%\ \text{DNA fragmentation} = [\text{OD}_{600}\ (\text{supernatant}) / (\text{OD}_{600}\ \text{supernatant} + \text{pellet})] \times 100$$

Qualitative DNA fragmentation (agarose gel electrophoresis)

Apoptotic DNA fragmentation was qualitatively assessed by agarose gel electrophoresis. SH-SY5Y cells (1×10^5 cells/well) were seeded in 6-well plates and treated with PQ (400 µM), BA (50 µM), Qe (50 µM), or their combinations for 48 h, while untreated cells served as control. Following treatment, both adherent and floating cells were collected, washed twice with PBS, and lysed in hypotonic lysis buffer on ice for 30 min. The lysates were centrifuged at 13,000 × g for 20 min at 4 °C to separate fragmented DNA (supernatant) from intact chromatin (pellet). DNA was purified by RNase A (0.1 mg/mL, 37 °C, 1 h) and proteinase K (0.2 mg/mL, 50 °C, 1 h) treatment, followed by isopropanol precipitation and resuspension in TE buffer.

Equal amounts of DNA (~ 500 ng–1 µg per lane) were loaded onto a 1.5% agarose gel prepared in 1× TAE buffer containing ethidium bromide (0.5 µg/mL). A 100 bp DNA ladder (Thermo Fisher Scientific) was used as a molecular marker. Electrophoresis was performed at 100 V for 60–90 min, and gels were visualized using a UV transilluminator. The appearance of a characteristic laddering pattern of ~ 180–200 bp and its multiples was considered indicative of apoptosis, whereas intact high-molecular-weight DNA in the control lane reflected preserved genomic integrity [31].

In Ovo HET-CAM (Hen's egg test Chorioallantoic Membrane) irritation test

The irritant effect of BA, Qe, PQ and their combinations was evaluated using the chorioallantoic membrane (CAM) of fertilized Leghorn hen eggs (50–60 g) according to the ICCVAM-recommended standard protocol [32, 33]. Fertilized eggs were incubated at 37 ± 1 °C and 80 ± 2% relative humidity for 7 days in an automatic incubator with rotation. On day 7, a window (3–4 cm in diameter) was carefully opened at the air chamber side of the shell, and the inner membrane was gently removed with forceps without damaging the underlying blood vessels.

Then, 300 µL of the freshly prepared PQ (2.5 mg/mL), BA (1 mg/mL), Qe (1 mg/mL), and their combinations were applied directly to the CAM surface pre-warmed to 37 °C. The CAM was then observed for 5-minutes, including the 20 s contact period, under constant illumination at room temperature.

Endpoints that should be observed were: Hemorrhage (bleeding from the vessels); Vascular lysis (blood vessel disintegration); Coagulation (intra- and extra-vascular protein denaturation).

The vascular responses (hyperemia, hemorrhage, coagulation) were scored according to their time of onset using the HET-CAM scoring system [32]:

Lysis: 5 (≤30 s), 3 (30 s–2 min), 1 (2–5 min)
Hemorrhage: 7 (≤30 s), 5 (30 s–2 min), 3 (2–5 min)
Coagulation: 9 (≤30 s), 7 (30 s–2 min), 5 (2–5 min)

For each egg, the irritation score (IS) was calculated as the sum of the three reactions. The final IS was expressed as the arithmetic mean of four eggs per group. Based on the French classification, IS values were interpreted as: 0.0–0.9: non-irritant; 1.0–4.9: mild irritant; 5.0–8.9: moderate irritant; 9.0–21.0: severe irritant. In addition, 0.9% NaCl was tested as a negative control and 0.1 N NaOH was tested as positive control. A mixture of four eggs was used for each test. All samples were tested in triplicate at different time points.

Statistical analysis

The statistical analysis was performed with SPSS 20.0 (SPSS, Chicago, IL, USA). Data were checked for normal distribution using the Shapiro–Wilk test and for homogeneity of variances using Levene's test, and both assumptions were satisfied before applying ANOVA. Both assumptions were satisfied with all datasets ($p > 0.05$). Differences between groups were analyzed using a one-way analysis of variance (ANOVA), followed by Tukey's post hoc test for multiple comparisons. All experiments were performed in triplicate, and data were expressed as mean ± standard deviation. Fold-change values are reported in the results for clarity, and the corresponding SD values are presented in the Supplementary Data for transparency. A p-value of less than 0.05 (≤ 0.05) was considered statistically significant.

Results

Cell viability and LDH assay

As shown in Fig. 1a, PQ significantly reduced viability to 34.3 ± 2.1% ($p < 0.05$) compared to control. BA (92.2 ± 5.1%, $p < 0.05$), Qe (93.4 ± 4.2%, $p < 0.05$) and BA + Qe (96.5 ± 4.0%, $p < 0.05$) significantly increased cell viability compared to the control (87.2 ± 1.5%). Combination treatments with BA + PQ (43.9 ± 2.6%, $p < 0.05$), Qe + PQ (49.5 ± 3.1%, $p < 0.05$) and BA + Qe + PQ (70.4 ± 4.0%, $p < 0.05$) significantly improved viability compared to PQ alone. Fluorescence microscopy supported these results, showing that PQ exposure led to pronounced nuclear condensation and fragmentation, characteristic of apoptotic damage. In contrast, treatment with BA, Qe, or their combination maintained predominantly intact, uniformly stained nuclei, consistent with preserved nuclear integrity (Fig. 1b).

As shown in Fig. 1c, the percentage of intact nuclei was 95.6 ± 2.1% in the control group. PQ exposure significantly reduced the percentage of intact nuclei to 29.3 ± 3.2% ($p < 0.05$). BA (92.4 ± 2.5%), Qe (93.8 ± 2.7%), and BA + Qe (96.2 ± 2.0%) maintained nuclear integrity comparable to control ($p > 0.05$). Combination treatments BA + PQ (49.3 ± 3.0%), Qe + PQ (53.4 ± 2.8%), and BA + Qe + PQ (78.5 ± 2.6%) significantly increased the proportion of intact nuclei compared with PQ alone ($p < 0.05$).

As seen in Fig. 2, PQ exposure significantly increased LDH release (40.3 ± 3.2 µU/mL) compared to control (5.9 ± 0.9 µU/mL, $p < 0.05$). BA (5.3 ± 1.1 µU/mL), Qe (6.0 ± 1.2 µU/mL) and BA + Qe (6.2 ± 1.3 µU/mL) showed no significant increase relative to control ($p > 0.05$). Co-treatment with BA + PQ (30.1 ± 2.2 µU/mL, $p < 0.05$), Qe + PQ (21.1 ± 1.8 µU/mL, $p < 0.05$) and BA + Qe + PQ (15.2 ± 1.6 µU/mL, $p < 0.05$) significantly reduced LDH levels compared to PQ.

Total antioxidant capacity (TAC) and total oxidative stress (TOS) activity

PQ significantly decreased ($p < 0.05$) TAC level (3.1 ± 0.4 mM) compared to control (6.1 ± 0.4 mM). BA (7.9 ± 0.5 mM, $p < 0.05$), Qe (9.4 ± 0.4 mM, $p < 0.05$) and BA + Qe (12 ± 0.6 mM, $p < 0.05$) significantly increased antioxidant levels compared to control. BA + PQ (4.3 ± 0.5 mM, $p < 0.05$), Qe + PQ (7.0 ± 0.7 mM, $p < 0.05$) and BA + Qe + PQ (8.6 ± 0.6 mM, $p < 0.05$) significantly improved TAC compared to PQ (Fig. 3a).

As seen Fig. 3b, PQ significantly elevated ($p < 0.05$) TOS level to 36 ± 2.0 µM compared to control (6.4 ± 0.7 µM). BA (6.0 ± 0.65 µM), Qe (6.6 ± 0.87 µM) and BA + Qe (5.9 ± 0.6 µM) treatments did not differ significantly ($p > 0.05$) from the control group. BA + PQ (30 ± 1.6 µM, $p < 0.05$), Qe + PQ (24 ± 1.5 µM, $p < 0.05$) and BA + Qe + PQ (15 ± 1.1 µM, $p < 0.05$) significantly reduced TOS compared to PQ.

ΔΨm changes

As shown in Fig. 4, PQ significantly increased ($p < 0.05$) fluorescence intensity (5000 ± 200 AU) compared to control (1000 ± 150 AU), indicating mitochondrial depolarization. BA (1000 ± 120 AU), Qe (1000 ± 120 AU) and BA + Qe (1100 ± 130 AU) did not significantly alter ΔΨm compared to control. BA + PQ (4000 ± 160 AU, $p < 0.05$), Qe + PQ (3900 ± 175 AU, $p < 0.05$) and BA + Qe + PQ (2000 ± 130 AU, $p < 0.05$) showed significantly lower ΔΨm values compared to PQ treatment.

Intracellular Ca^{2+} levels

As shown in Fig. 5, PQ significantly increased intracellular Ca^{2+} to 75.2 ± 1.5 ng/10^6 cells compared to control (12 ± 0.62 ng/10^6 cells, $p < 0.05$). BA (13.2 ± 0.41

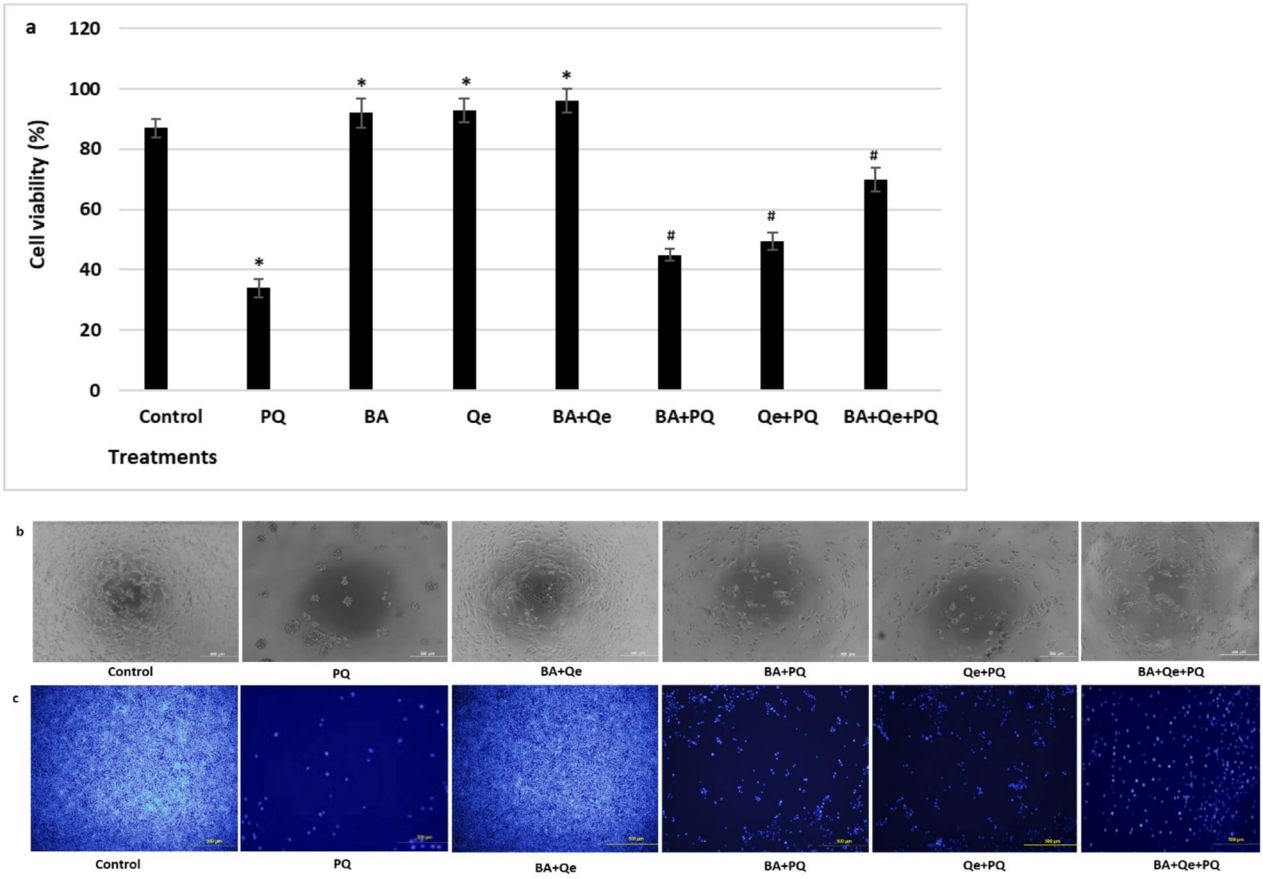

Fig. 1 Cell viability (%) (**a**), morphological changes (**b**), fluorescence photomicrographs of DAPI staining (blue) **(c)** in SH-SY5Y cells (scale bars: 500 µM). Data are expressed as % of control (mean ± SD, $n = 3$). *$p < 0.05$ compared to the control; #$p < 0.05$ compared to the PQ. PQ: Paraquat, Qe: Quercetin, BA: Boric acid

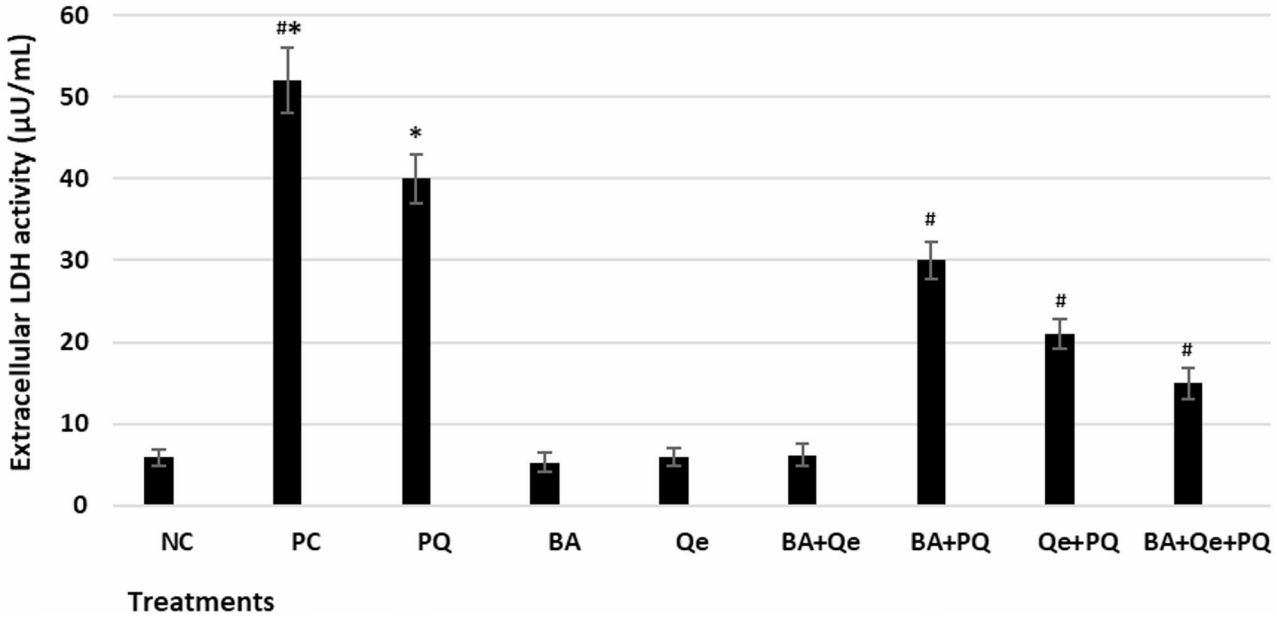

Fig. 2 Extracellular LDH activity (µU/mL) in SH-SY5Y cells after treatment with BA (50 µM), Qe (50 µM), PQ (400 µM) and their combination for 48 h. Data are expressed as % of total LDH (mean ± SD, $n = 3$). *$p < 0.05$ compared to the control; #$p < 0.05$ compared to the PQ. NC: Negative control, PC: Positive control as H_2O_2 for LDH (2.5×10^{-5} M). PQ: paraquat, Qe: quercetin, BA: boric acid

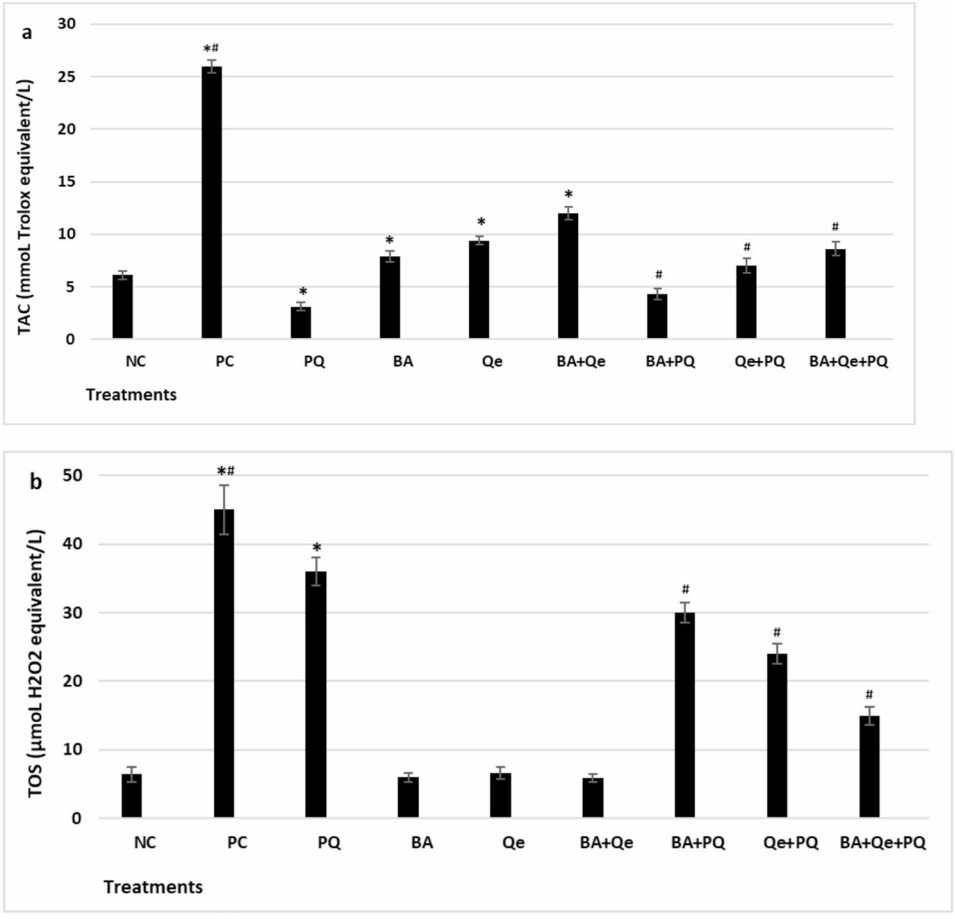

Fig. 3 Total antioxidant status (TAC) (**a**) and total oxidative stress (TOS) (**b**) after treatment with BA (50 µM), Qe (50 µM), PQ (400 µM) and their combination in SH-SY5Y cells for 48 h. Values represent mean ± SD of at least three experiments. *$p < 0.05$ compared to the control; #$p < 0.05$ compared to the PQ. NC: Negative control, PC: Positive control as ascorbic acid (10^{-5} M) for TAC and H_2O_2 (2.5×10^{-5} M) for TOS. PQ: Paraquat, Qe: Quercetin, BA: Boric acid

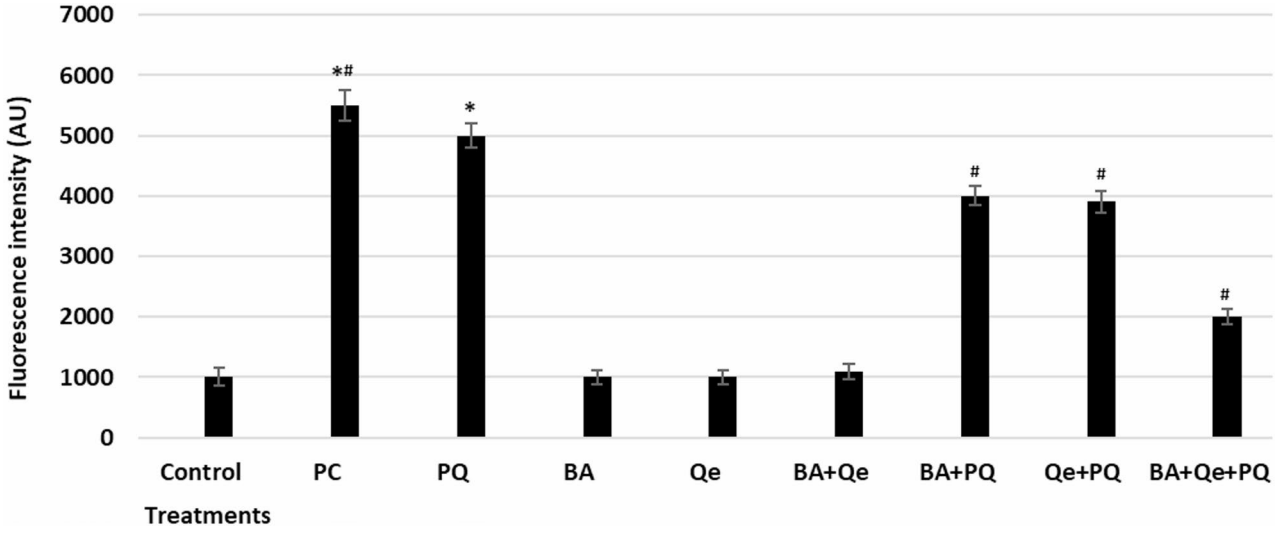

Fig. 4 Quantitative analysis of mitochondrial membrane potential (ΔΨm) after treatment with BA (50 µM), Qe (50 µM), PQ (400 µM) and their combinations in SH-SY5Y cells. Data are presented as relative fluorescence intensity (% of control). Values represent mean ± SD of at least three experiments. *$p < 0.05$ compared to the control; #$p < 0.05$ compared to the PQ. PC: Carbonyl cyanide 3-chlorophenylhydrazone (CCCP) was used as positive control (10 µM). PQ: Paraquat, Qe: Quercetin, BA: Boric acid

ng/10^6 cells), Qe (12.5 ± 0.52 ng/10^6 cells) and BA + Qe (12.1 ± 0.44 ng/10^6 cells) were similar to control ($p > 0.05$). BA + PQ (50.3 ± 1.3 ng/10^6 cells, $p < 0.05$), Qe + PQ (45.2 ± 1.1 ng/10^6 cells, $p < 0.05$) and BA + Qe + PQ (22.1 ± 0.8 ng/10^6 cells, $p < 0.05$) significantly reduced intracellular Ca^{2+} level compared to PQ (75.2 ± 1.5 ng/10^6).

SOD, GPx and MDA values

As shown in Fig. 6a, PQ (65 ± 2.1 U/mg protein) significantly decreased ($p < 0.05$) compared to control (105.2 ± 4.3 U/mg protein). BA (132.3 ± 4.4 U/mg protein, $p < 0.05$), Qe (140.3 ± 4.6 U/mg protein, $p < 0.05$) and BA + Qe (177 ± 6.2 U/mg protein, $p < 0.05$) significantly increased compared to control. BA + PQ (101 ± 3.2 U/mg protein, $p < 0.05$), Qe + PQ (121.3 ± 4.2 U/mg protein, $p < 0.05$) and BA + Qe + PQ (151.2 ± 5.8 U/mg protein, $p < 0.05$) increased compared to PQ.

As seen in Fig. 6b, PQ (20.1 ± 2 mU/mg protein) significantly decreased ($p < 0.05$) compared to control (60.2 ± 4 mU/mg protein). BA (68.3 ± 5.2 mU/mg protein, $p < 0.05$), Qe (73.3 ± 6.1 mU/mg protein, $p < 0.05$) and BA + Qe (80.4 ± 5.7 mU/mg protein, $p < 0.05$) significantly increased compared to control. BA + PQ (32.2 ± 2.8 mU/mg protein, $p < 0.05$), Qe + PQ (40.3 ± 2.4 mU/mg protein, $p < 0.05$) and BA + Qe + PQ (50.1 ± 3 mU/mg protein, $p < 0.05$) significantly increased compared to PQ.

As seen in Fig. 6c, PQ (4.00 ± 0.09 nmol/mg protein) significantly increased ($p < 0.05$) compared to control (1.27 ± 0.03 nmol/mg protein). BA (1.30 ± 0.07 nmol/mg protein, $p > 0.05$), Qe (1.26 ± 0.06 nmol/mg protein, $p > 0.05$) and BA + Qe (1.32 ± 0.09 nmol/mg protein, $p > 0.05$) showed no significant change compared to control. BA + PQ (2.80 ± 0.10 nmol/mg protein, $p < 0.05$), Qe + PQ (3.20 ± 0.09 nmol/mg protein, $p < 0.05$) and BA + Qe + PQ (2.10 ± 0.14 nmol/mg protein, $p < 0.05$) significantly decreased compared to PQ.

Gene expression levels

As shown in Fig. 7, the expression of genes related to inflammation (TNF, IL-1β, NFKB1, TRAF1), apoptosis (BAX, BCL2, CASP3, TP53), angiogenesis (VEGF, MMP9) and oxidative stress (NRF2) was significantly modulated by PQ, BA, Qe and their combinations in SH-SY5Y cells.

Treatment with PQ increased TNF expression (5.0-fold change), indicating a strong inflammatory response. BA + Qe led to a downregulation (0.4-fold change), indicating synergistic anti-inflammatory effects. PQ + BA and PQ + Qe reduced TNF levels compared to PQ alone (2.0-fold and 1.5-fold change, respectively). PQ + BA + Qe brought TNF expression back to a near control level (0.8-fold change), indicating a strong attenuation of PQ-induced inflammation.

PQ increased TRAF1 expression with a 2.5-fold change, indicating activation of TNF-related apoptotic signalling. PQ + BA and PQ + Qe decreased TRAF1 expression by 1.6- and 1.3-fold, respectively, compared to PQ alone. PQ + BA + Qe reduced TRAF1 expression to a 0.9-fold change compared to PQ alone, indicating a reversal of PQ-induced activation of the signalling pathway.

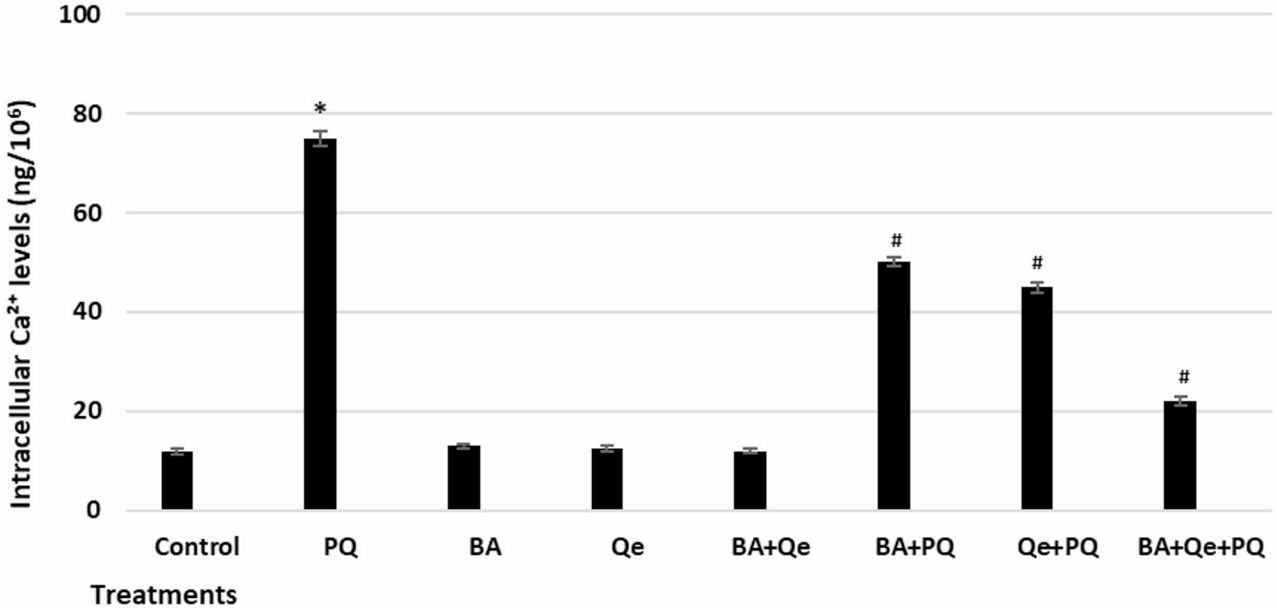

Fig. 5 Changes in intracellular Ca^{2+} concentrations (ng/106 cells) in SH-SY5Y exposed to BA (50 µM), Qe (50 µM), PQ (400 µM) and their combinations for 48 h. Values represent mean ± SD of at least three experiments. *$p < 0.05$ compared to the control; #$p < 0.05$ compared to the PQ. PQ: Paraquat, Qe: Quercetin, BA: Boric acid

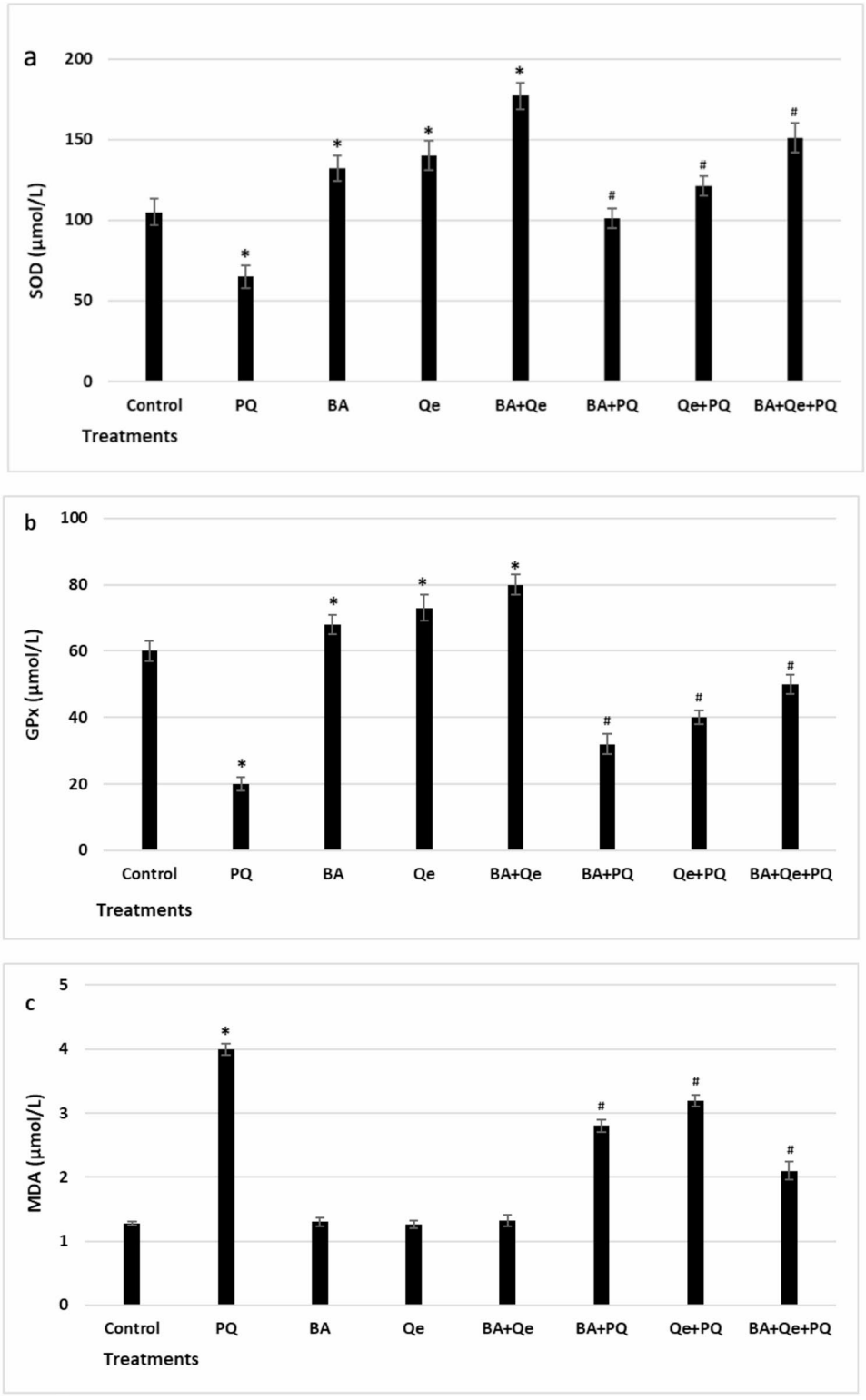

Fig. 6 Superoxide dismutase (SOD) (**a**), glutathione peroxidase (GPx) (**b**) and malondialdehyde (MDA) (**c**) after treatment with BA (50 µM), Qe (50 µM), PQ (400 µM) and their combination in SH-SY5Y cells. Values represent mean ± SD of at least three experiments. *$p < 0.05$ compared to the control; #$p < 0.05$ compared to the PQ. PQ: Paraquat, Qe: Quercetin, BA: Boric acid

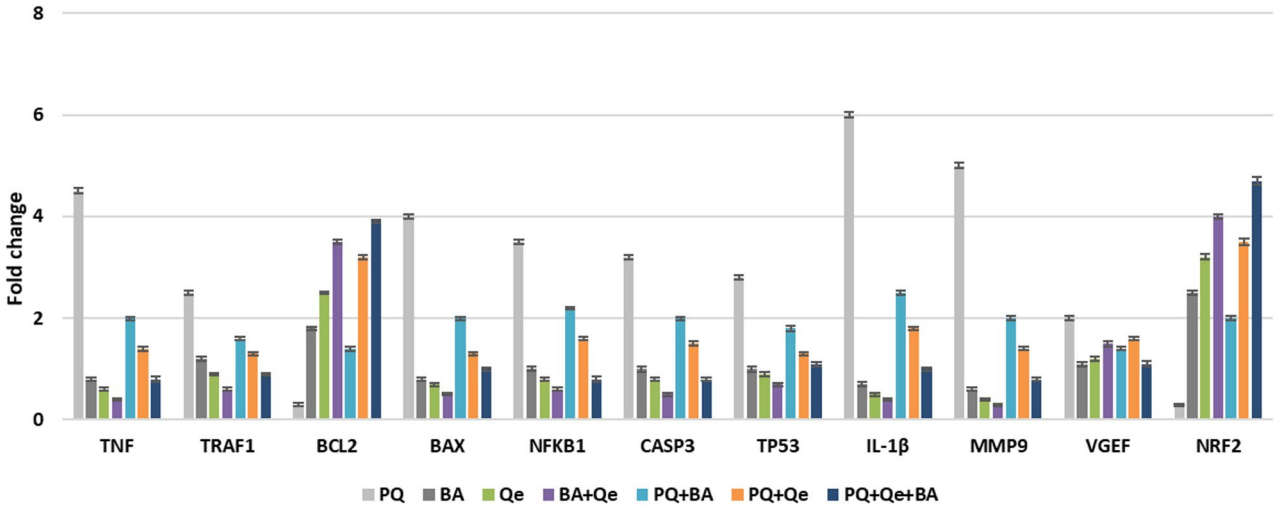

Fig. 7 Fold changes in gene expression levels in cell lines exposed to BA (50 µM), Qe (50 µM), PQ (400 µM) and their combination in SH-SY5Y cells using real-time quantitative PCR (qRT-PCR). Relative expressions were calculated using the $2^{-\Delta\Delta Ct}$ method and normalized to β-actin as an internal control. Values represent mean ± SD of at least three experiments. PQ: Paraquat, Qe: Quercetin, BA: Boric acid

PQ caused a strong pro-apoptotic response by upregulating BAX (4.0-fold change). BA, Qe and BA + Qe reduced BAX expressions to 0.8-, 0.7- and 0.5-fold, respectively. Treatment with PQ + Qe + BA reduced BAX expression with a value of 0.7, indicating apoptotic suppression.

The anti-apoptotic BCL2 was downregulated by PQ (0.3-fold). BA, Qe and BA + Qe increased BCL2 expression (1.8-, 2.5- and 3.4-fold change, respectively). PQ + Qe + BA significantly increased BCL2 expression by 4.5-fold, reversing the PQ-induced apoptotic imbalance.

PQ increased caspase-3 expression by 3.2-fold, indicating apoptotic execution. BA + Qe upregulated the expression of caspase-3 by 0.5-fold. PQ + BA and PQ + Qe reduced caspase-3 expression by 2-fold and 1.5-fold, respectively, compared to PQ alone. PQ + Qe + BA reduced caspase-3 expression by 0.8-fold, indicating effective apoptosis inhibition.

PQ induced IL-1β expression with a value of 6-fold change, consistent with cytokine storm-like inflammation. BA, Qe and BA + Qe reduced IL-1β expression with a 0.7-, 0.5- and 0.4-fold change, respectively. Concomitant treatment with PQ + BA + Qe significantly reduced IL-1β expression compared to PQ alone, suggesting anti-inflammatory protection.

PQ increased the expression of NFκB1 with a 3.5-fold change, indicating inflammatory activation. PQ + BA, PQ + Qe and PQ + Qe + BA decreased expression by 2.2-, 1.6- and 0.8-fold, respectively, compared to PQ alone, indicating a complete attenuation of NFκB1-mediated signalling.

PQ resulted in a significant increase in MMP9 with a 5.0-fold change, indicating extracellular matrix degradation and tissue injury. BA, Qe and BA + Qe decreased MMP9 (0.6-, 0.4- and 0.3-fold change, respectively). PQ + BA, PQ + Qe and PQ + Qe + BA decreased expression with a 2-, 1.4- and 0.8-fold change, respectively, compared to PQ alone, restoring baseline levels and indicating tissue-protective effects.

PQ increased VEGF expression with a 2.0-fold change, indicating angiogenic stress. BA, Qe and BA + Qe increased VEGF expression by 1.1-, 1.2- and 1.5-fold, respectively. PQ + BA, PQ + Qe and PQ + Qe + BA decreased VEGF expression with a 1.4-, 1.6- and 1.1-fold change compared to PQ alone, restoring baseline levels and indicating tissue-protective effects.

PQ increased TP53 levels by 2.8-fold, indicating a response to DNA damage. Qe and BA + Qe downregulated TP53 expression with a 0.9- and 0.7-fold change, respectively. PQ + BA, PQ + Qe and PQ + Qe + BA reduced TP53 expression by 1.8-, 1.3- and 1.1-fold, respectively, compared to PQ alone, indicating protection against genotoxic stress.

PQ reduced NRF2 expression with a 0.3-fold change, indicating susceptibility to oxidative stress. BA, Qe and BA + Qe increased NRF2 with a 2.5-, 3.2- and 4-fold change, respectively). PQ + BA, PQ + Qe and PQ + Qe + BA increased NRF2 expressions by 2-, 3.5- and 4.7-fold, respectively, compared to PQ alone, indicating a strong activation of the antioxidant response.

DNA fragmentation

As seen in Fig. 8a, PQ (65.3 ± 1.5%) significantly increased ($p < 0.05$) DNA fragmentation compared to control (7.2 ± 0.62%). BA (9.2 ± 0.41%, $p > 0.05$), Qe (8.1 ± 0.52%, $p > 0.05$) and BA + Qe (9.5 ± 0.44%, $p > 0.05$) did not differ from control. BA + PQ (40.3 ± 0.9%, $p < 0.05$), Qe + PQ

(35 ± 1.1%, $p < 0.05$) and BA + Qe + PQ (20.1 ± 0.8%, $p < 0.05$) were significantly lower compared to PQ.

As shown in the agarose gel image (Fig. 8b), PQ treatment induced a clear DNA laddering pattern, indicating extensive apoptotic fragmentation, whereas the control, BA + Qe group exhibited intact high-molecular-weight DNA bands with no visible fragmentation. Co-treatment with BA or Qe partially reduced PQ-induced laddering, consistent with moderate levels of fragmentation, while the triple combination (BA + Qe + PQ) markedly preserved DNA integrity, showing only faint or minimal laddering compared to PQ alone. The raw SDS-PAGE gel image is provided in the supplementary file.

In Ovo HET-CAM assay

The effects of irritation on vascularization after exposure to PQ, Qe, BA and their combination are shown in Fig. 9. PQ caused hemorrhage and lysis as well as severe irritation with an IS of 9.1 ± 0.2 for a period of up to 5-minutes. BA, Qe and BA + Qe had no irritating effect. BA + PQ, Qe + PQ caused moderate irritation with an IS of 6.2 ± 0.1 and 6 ± 0.2, respectively, while BA + Qe + PQ caused mild irritation with an IS of 4.1 ± 0.2.

Discussion

This study demonstrated that the co-administration of BA and Qe effectively alleviated the neurotoxic effects of PQ in SH-SY5Y. These protective effects were facilitated by mitochondrial stabilization, restoration of Ca^{2+} homeostasis, enhancement of antioxidant defense mechanisms, and attenuation of both inflammatory and apoptotic signaling pathways. PQ increases ROS and disrupts several key cellular processes critical for neuronal survival. Its effects on mitochondrial activity, genomic stability, and membrane integrity are closely linked to synaptic dysfunction and neuronal loss [34].

In this model, PQ exposure led to a marked decrease in cell viability, along with a decrease in TAC and an increase TOS. These findings are consistent with previous studies in neuroblastoma and non-neuronal cell lines reporting concentration- and time-dependent cytotoxicity [35–37]. The observed decline in TAC, increase in TOS, and LDH release reflected ROS-driven cell damage, which is known to be facilitated by redox enzymes such as cytochrome P450 oxidoreductase [38–40]. Mitochondria played a crucial role in this damage pathway, as PQ disrupted their function, elevated ROS production, and depolarized the inner mitochondrial membrane, thereby promoting apoptosis [41–43]. Consistent with these findings, PQ exposure in SH-SY5Y cells resulted in increased LDH release, decreased cell viability, loss of ΔΨm, and elevated ROS production.

One key mechanistic pathway identified was the relationship between mitochondrial integrity and Ca^{2+} regulation. PQ disrupts intracellular Ca^{2+} regulation by oxidatively modifying key transport proteins, including plasma membrane Ca^{2+}-ATPase and sarco/endoplasmic reticulum Ca^{2+}-ATPase, resulting in increased Ca^{2+} influx and impaired sequestration [44]. Excess mitochondrial Ca^{2+}, combined with ROS, triggers the opening of the mitochondrial permeability transition pore (mPTP), resulting in mitochondrial depolarisation, swelling, and the release of pro-apoptotic factors such as cytochrome c, Smac/DIABLO, and AIF, ultimately initiating intrinsic apoptosis [45, 46]. In the present study, the combination of BA and Qe reduced PQ-induced Ca^{2+} accumulation and alleviated the loss of ΔΨm. These findings suggest enhanced mitochondrial buffering capacity and delayed opening of the mitochondrial permeability transition

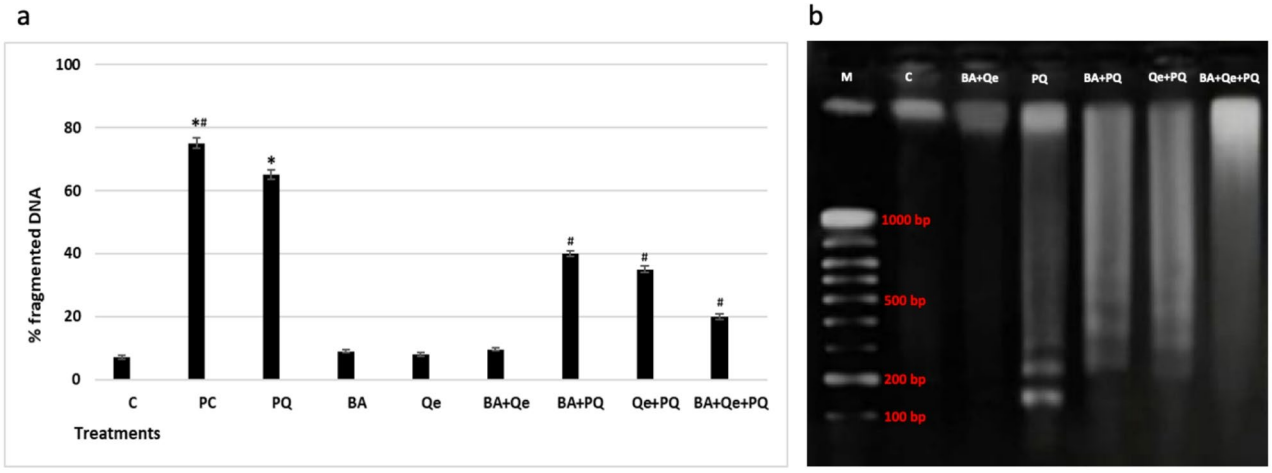

Fig. 8 DNA fragmentation rate (**a**) and representative gel electrophoresis image of DNA laddering (**b**) formed by BA (50 µM), Qe (50 µM), PQ (400 µM) and their combination in SH-SY5Y. Values represent mean ± SD of at least three experiments. *$p < 0.05$ compared to the control; #$p < 0.05$ compared to the PQ. PQ: Paraquat, Qe: Quercetin, BA: Boric acid

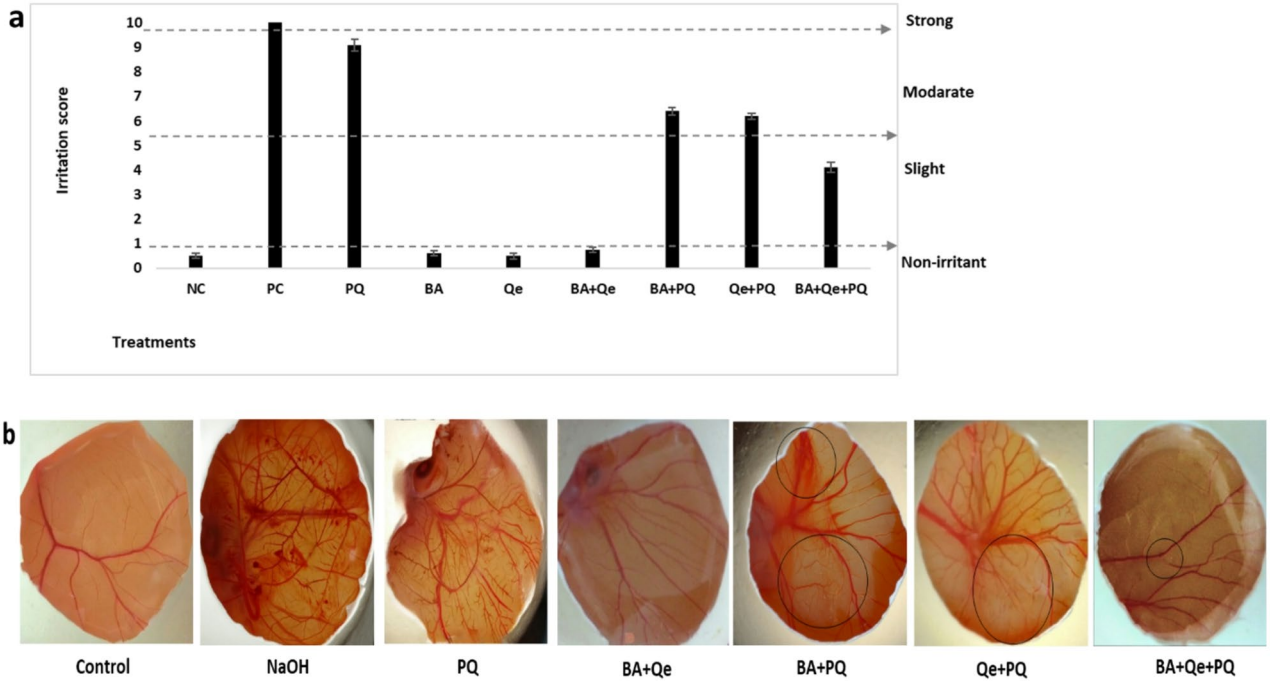

Fig. 9 HET-CAM assay. (**a**) Irritation values after treatment with BA, Qe, PQ and their combination on the membrane surface for up to 5-minutes using the HET-CAM test. (**b**) Pictures indicating how various endpoints on the membrane following BA, Qe, PQ and their combination. Values represent mean ± SD of at least three experiments. PQ: Paraquat, Qe: Quercetin, BA: Boric acid. NaCl (0.9%) and NaOH (0.1 N) used as negative and positive control, respectively

pore (mPTP). This indicates improved mitochondrial buffering capacity and delayed opening of the mitochondrial permeability transition pore (mPTP) [47].

A second major finding was the activation of the antioxidant defense system, accompanied by a decrease in lipid peroxidation. PQ-induced superoxide production initially triggered an adaptive increase in SOD and GPx activity. However, extended exposure led to the depletion of these enzymes and resulted in membrane damage. Consistent with previous research, BA treatment reduced LDH release and MDA levels, while restoring TAC and antioxidant enzyme activity under oxidative stress [48–54]. Qe showed similar protective effects, ameliorating PQ-induced cytotoxicity and reducing lipid peroxidation [55–57]. The distinct but synergistic antioxidant properties of BA and Qe likely contributed to the enhanced protective effect observed when used together.

At the gene expression level, PQ activates inflammatory pathways. This includes the activation of NF-κB signaling and TNF receptor-associated factors such as TRAF1 [25, 58–60]. In the current study, BA reduced the expression of key pro-inflammatory and angiogenic genes. This effect was more obvious when combined with Qe, particularly for genes such as NFKB, TNF, TRAF1, and VEGF. Simultaneously, apoptotic markers such as BAX and Caspase-3 were downregulated, while anti-apoptotic BCL2 expression increased. Additionally, the combination treatment led to enhanced activation of NRF2. This finding was consistent with the observed improvements in antioxidant parameters. This observation also highlights the antagonistic relationship between NRF2 activation and NF-κB-mediated cytokine expression [60, 61]. Previous studies have demonstrated PQ-induced upregulation of pro-apoptotic genes like BAX, Caspase-3, and p53, along with modulation of BCL2 in brain and lung tissues [62–65]. PQ-associated oxidative stress was also linked to alterations in the PTEN/PI3K/AKT pathway [66]. Although the anticancer activity of BA is believed to involve inhibition of AKT signaling [67], the potential role of it in modulating the PTEN/PI3K/AKT pathway in the context of chemical neurotoxicity had not been previously studied. This underscores the novelty and significance of the present gene expression findings. Importantly, Qe formulations have also demonstrated protective effects in previous studies. For instance, under PQ-induced stress, they reversed the loss of ΔΨm and normalized BAX/BCL2 expression levels [68].

The genoprotective effects observed in this study further support the early-stage modulations induced by BA and Qe. Treatment significantly reduced PQ-induced DNA fragmentation. Agarose gel electrophoresis of genomic DNA also showed a significant reduction in PQ-induced fragmentation in samples treated with BA and Qe. Specifically, co-treatment with BA or Qe preserved DNA integrity by reducing the characteristic DNA laddering and smearing observed with PQ alone. Previous

research has shown that BA activates PERK-dependent eIF2α/NRF2 signaling, which promotes DNA repair and mitigates genotoxicity [22, 69]. Also, Qe mitigated ROS-induced cell damage by preserving mitochondrial integrity and inhibiting caspase-3 activation, ultimately preventing DNA fragmentation [70]. In addition, Qe enhanced endogenous antioxidant systems, including GSH and SOD, thereby contributing to a less oxidative and more protective intracellular environment [71]. Collectively, these findings indicate that BA facilitates DNA repair, whereas Qe prevents the onset of oxidative damage. Together, they provide synergistic genoprotective effects under conditions of oxidative stress.

The HET-CAM test utilizes the highly vascularized CAM to effectively assess irritant effects, particularly those related to inflammation and vascular damage. In this study, PQ exposure induced marked hemorrhage, lysis, and coagulation responses on the CAM, reflecting substantial vascular irritation and inflammation [72]. These findings align with the established neurotoxic profile of PQ, in which oxidative stress and inflammation play a crucial role in mediating neuronal damage [73]. In neuronal tissues such as SH-SY5Y cells, PQ-induced oxidative stress disrupts mitochondrial function, elevates ROS production, and initiates neuronal apoptosis, often in conjunction with inflammatory activation and endothelial dysfunction. VEGF is a critical regulator of vascular permeability and neurovascular remodeling, and it was significantly upregulated in the PQ-treated group. VEGF is not only a marker of endothelial activation, but also plays an essential role in neuroinflammation and blood-brain barrier disruption both of which are relevant to PQ-induced central nervous system toxicity [74]. The increased expression of VEGF demonstrates that PQ exposure promotes inflammatory neovascular signaling and may contribute to blood-brain barrier breakdown and neuronal damage. In contrast, treatment with BA and Qe, either individually or in combination, resulted in a significant reduction in irritation levels in the HET-CAM assay. Notably, the group with simultaneous treatment (BA + Qe + PQ) showed the most apparent protective effect, indicating a possible synergistic effect. This outcome is likely due to the combined antioxidant and anti-inflammatory properties of BA and Qe, with BA modulating inflammatory signaling pathways and Qe enhancing endogenous antioxidant defense mechanisms by upregulating enzymes such as GPx and SOD. Gene expression analysis confirmed these observations, showing that combined treatment with BA and Qe significantly reduced VEGF expression compared to the PQ group, bringing levels close to baseline. This suggests a suppression of oxidative stress-induced vascular and neuroinflammatory responses. Overall, these results suggest that co-administration of BA and Qe attenuates PQ-induced neurovascular damage by stabilizing endothelial function, reducing oxidative stress, and inhibiting VEGF-mediated pro-inflammatory signaling. The convergence of the HET-CAM results and VEGF gene expression highlights the translational relevance of the combined BA and Qe approach in mitigating paraquat-induced neurotoxic and vasculopathic effects.

This study provides comprehensive evidence for the protective role of BA and Qe against PQ-induced neurotoxicity, while also outlining directions for future work to enhance translational impact. Our mechanistic analyses focused on mRNA expression, offering valuable insights into transcriptional regulation; however, complementary protein-level validation (e.g., Western blotting) would strengthen the mechanistic interpretation. Although SH-SY5Y cells and the *in ovo* HET-CAM assay are well-established neuronal and vascular models, they can't fully capture the systemic complexity of mammalian brain tissue or long-term neurovascular interactions. The 5-minutes observation window used in the HET-CAM assay follows the ICCVAM-recommended standard and ensures comparability with previous reports, yet longer observation periods could further reveal the persistence or recovery of vascular responses.

In conclusion, considerations such as bioavailability, metabolism, and safe dosing of BA and Qe highlight the importance of follow-up studies in animal models that integrate behavioral, neurovascular, and pharmacokinetic outcomes to bridge towards clinical translation.

Conclusions

This study demonstrates, for the first time, that BA protects neuronal cells against PQ-induced neurotoxicity and that its combination with Qe provides synergistic protection. The co-treatment effectively attenuated oxidative stress, preserved mitochondrial integrity, restored Ca^{2+} homeostasis, and modulated apoptosis- and inflammation-related gene expression in SH-SY5Y cells. In addition, the *in ovo* HET-CAM assay confirmed the translational relevance of these findings by displays that BA and Qe, especially in combination, reduce PQ-induced vascular irritation and VEGF upregulation.

Importantly, BA significantly improved cell viability in the presence of Qe, suggesting that the two compounds can regenerate each other and provide stronger overall protection against PQ-induced cellular damage, consistent with a synergistic mechanism of action. Overall, our results highlight BA and Qe as promising complementary therapeutic agents to counteract PQ-induced oxidative, apoptotic, and inflammatory damage. Future studies in animal models and clinical systems are needed to evaluate the long-term safety, bioavailability, pharmacokinetics, and efficacy of BA and Qe. Additionally, these studies should assess their potential use in preventive or adjunctive therapies for chemically induced neural injury.

Supplementary Information

The online version contains supplementary material available at https://doi.org/10.1186/s12906-025-05199-w.

Supplementary Material 1.

Authors' contributions

AG: Supervision, Conceptualization, Methodology, Writing – Original Draft.AT: Methodology, Writing – Original Draft, Data curation, Formal analysis.

Funding

This research received no external funding.

Data availability

All data generated or analysed during this study are available from the corresponding author on reasonable request.

Declarations

Ethics approval and consent to participate

Not applicable.

Consent for publication

Not applicable.

Competing interests

The authors declare no competing interests.

Author details

[1]Faculty of Health Sciences, Department of Occupational Health and Safety, Sinop University, Sinop, Turkey
[2]Şebinkarahisar Vocational School of Health Services, Department of Statistics, Giresun University, Giresun, Turkey

Received: 10 August 2025 / Accepted: 25 November 2025
Published online: 01 December 2025

References

1. Huang Y, Zhan H, Bhatt P, Chen S. Paraquat degradation from contaminated environments: current achievements and perspectives. Front Microbiol. 2019;10:1754. https://doi.org/10.3389/fmicb.2019.01754.
2. Roberts TR, Dyson JS, Lane MCG. Deactivation of the biological activity of paraquat in the soil environment: A review of long-term environmental fate. J Agric Food Chem. 2002;50:3623–31.
3. Bang YJ, Kim J, Lee WJ. Paraquat use among farmers in Korea after the ban. Arch Environ Occup Health. 2017;72:231–4. https://doi.org/10.1080/19338244.2016.1192982.
4. Han JF, Wang SL, He X, Liu CY, Hong J. Effect of genetic variation on human cytochrome P450 reductase-mediated paraquat cytotoxicity. Toxicol Sci. 2006;91:42–8.
5. Cha ES, Chang SS, Gunnell D, Eddleston M, Khang YH, Lee WJ. Impact of paraquat regulation on suicide in South Korea. Int J Epidemiol. 2016;45:470–9. https://doi.org/10.1093/ije/dyv304.
6. Navneet A, Wadhera S, Dhibar PD. Paraquat poisoning: what we do and do not know. J Clin Toxicol. 2021;9:004.
7. See WZC, Naidu R, Tang KS. Cellular and molecular events leading to paraquat-induced apoptosis: Mechanistic insights into Parkinson's disease pathophysiology. Mol Neurobiol. 2021;59:3353–69. https://doi.org/10.1007/s12035-022-02799-2.
8. Blanco-Ayala T, Andérica-Romero AC, Pedraza-Chaverri J. New insights into antioxidant strategies against paraquat toxicity. Free Radic Res. 2014;48:623–40. https://doi.org/10.3109/10715762.2014.899694.
9. Liu Z, Wang X, Wang Y, et al. NLRP3 inflammasome activation regulated by NF-κB and DAPK contributed to paraquat-induced acute kidney injury. Immunol Res. 2017;65:687–698. https://doi.org/10.1007/s12026-017-8901-7.
10. Kavianinia M, Kalantar H, Salehcheh M, et al. Dimethyl fumarate effects on paraquat-induced hepatotoxicity in mice via anti-oxidative, anti-inflammatory, and anti-apoptotic activities. Sci Rep. 2025;15:3897. https://doi.org/10.1038/s41598-025-88461-y.
11. Gupta SV, Campos L, Schmidt KH. Mitochondrial superoxide dismutase Sod2 suppresses nuclear genome instability during oxidative stress. Genetics. 2023;225:iyad147. https://doi.org/10.1093/genetics/iyad147.
12. Yang W, Tiffany-Castiglioni E. The bipyridyl herbicide Paraquat produces oxidative stress-mediated toxicity in human neuroblastoma SH-SY5Y cells: relevance to the dopaminergic pathogenesis. J Toxicol Environ Health Part Taylor Francis. 2005;68:1939–61. https://doi.org/10.1080/15287390500226987.
13. Ahmed A, Prasad A, Bhattacharjee A. Management of paraquat poisoning—the way forward. Indian J Crit Care Med Jaypee Brothers Med Publishing. 2024;28:722–3. https://doi.org/10.5005/jp-journals-10071-24781.
14. Boots AW, Haenen GRMM, Bast A. Health effects of quercetin: from antioxidant to nutraceutical. Eur J Pharmacol. 2008;585:325–37. https://doi.org/10.1016/j.ejphar.2008.03.008.
15. Yılmaz S, Ustundag A, Cemiloglu Ulker O, Duydu Y. Protective effect of boric acid on oxidative DNA damage in Chinese hamster lung fibroblast V79 cell lines. Cell J (Yakhteh). 2016;17:748–54. https://doi.org/10.22074/cellj.2016.3847.
16. Jin Z, Ke J, Guo P, Wang Y, Wu H. Quercetin improves blood-brain barrier dysfunction in rats with cerebral ischemia reperfusion via Wnt signaling pathway. Am J Transl Res. 2019;11 IS 8:4683–95.
17. Zhang X, Wang G, Chen S. Boric acid alleviates lipopolysaccharide-induced acute lung injury in mice. Biol Trace Elem Res. 2025;203:1494–501. https://doi.org/10.1007/s12011-024-04240-2.
18. Ataizi ZS, Özkoç M, Kanbak Güngör, Karimkhani H, Donmez DB, Ustunisik N, et al. Evaluation of the neuroprotective role of boric acid in preventing traumatic brain injury-mediated oxidative stress. Turkish Neurosurg. 2019. https://doi.org/10.5137/1019-5149.JTN.25692-18.5.
19. Ceyhan Hacioglu F, Kar H, Senturk. Güngör Kanbak. Neuroprotective effects of boric acid against fluoride toxicity on rat synaptosomes. Med Sci Discovery. 2018;5:260–6. https://doi.org/10.17546/MSD.443140.
20. Yongjie Xiong E, Jin Q, Yin C, Che S, He. Boron attenuates heat stress-induced apoptosis by inhibiting endoplasmic reticulum stress in mouse granulosa cells. Biol Trace Elem Res. 2021;199:611–21. https://doi.org/10.1007/S12011-020-02180-1.
21. Özdemir Ç, Mustafa Arslan A, Küçük Z, Yığman A, Dursun. Therapeutic efficacy of boric acid treatment on brain tissue and cognitive functions in rats with experimental Alzheimer's disease. Drug Des Dev Therapy. 2023;17:1453–62. https://doi.org/10.2147/DDDT.S405963.
22. Kristin Yamada CD, Eckhert. Boric acid activation of eIF2α and Nrf2 is PERK dependent: a mechanism that explains how boron prevents DNA damage and enhances antioxidant status. Biol Trace Elem Res. 2019;188:2–10. https://doi.org/10.1007/S12011-018-1498-4.
23. Tekin A, Güner A, Akkan T. Protective effect of boric acid against ochratoxin A-induced toxic effects in human embryonal kidney cells (HEK293): a study on cytotoxic, genotoxic, oxidative, and apoptotic effects. Biol Trace Elem Res. 2025;203:810–21. https://doi.org/10.1007/s12011-024-04194-5.
24. Carneiro P, Ferreira M, Marisa Costa V, Carvalho F, Capela JP. Protective effects of amphetamine and methylphenidate against dopaminergic neurotoxicants in SH-SY5Y cells. Curr Res Toxicol. 2024;6:100165. https://doi.org/10.1016/j.crtox.2024.100165.
25. Yang W, Tiffany-Castiglioni E, Lee MY, Son IH. Paraquat induces cyclooxygenase-2 (COX-2) implicated toxicity in human neuroblastoma SH-SY5Y cells. Toxicol Lett. 2010;199:239–46. https://doi.org/10.1016/j.toxlet.2010.09.005.
26. Ayna A, Özbolat SN, Darendelioglu E. Quercetin, chrysin, caffeic acid and ferulic acid ameliorate cyclophosphamide-induced toxicities in SH-SY5Y cells. Mol Biol Rep. 2020;47:8535–43. https://doi.org/10.1007/s11033-020-05896-4.
27. Pakrashi S, Chakraborty J, Bandyopadhyay J. Quercetin alleviates 6-OHDA-caused apoptosis in SH-SY5Y cells. Toxicol Res. 2024;13:tfae117. https://doi.org/10.1093/toxres/tfae117.
28. Okudan Altındaş MD, Güner A. Astaxanthin attenuates chlorpyrifos-induced pulmonary cytotoxicity by modulating mitochondrial redox and inflammatory pathways. Curr Issues Mol Biol. 2025;47. https://doi.org/10.3390/cimb47080663.
29. Güner A, İlhan S. Cytotoxic, genotoxic, oxidative, and irritant effects of zinc pyrithione in vitro. Toxicol Environ Chem Taylor Francis. 2020;102:607–23. https://doi.org/10.1080/02772248.2020.1824258.
30. Burton K. A study of the conditions and mechanism of the diphenylamine reaction for the colorimetric estimation of deoxyribonucleic acid. Biochem J. 1956;62:315–23. https://doi.org/10.1042/bj0620315.
31. Herrmann M, Lorenz HM, Voll R, Griinke M, Woith W, Kalden JR. A rapid and simple method for the isolation of apoptotic DNA fragments. Nucleic Acids Res. 1994;22:5506–7. https://doi.org/10.1093/nar/22.24.5506.

32. .Luepke N. Hen's egg chorioallantoic membrane test for irritation potential. Food Chem Toxicol. 1985;23:287–291.
33. National Institutes of Health (NIH). ICCVAM test method evaluation report: current validation status of. In vitro test methods proposed for identifying eye injury hazard potential of chemicals and products. Interagency Coordinating Committee on the Validation of Alternative Methods (ICCVAM); 2010.
34. Chen J, Su Y, Lin F, Iqbal M, Mehmood K, Zhang H, et al. Effect of paraquat on cytotoxicity involved in oxidative stress and inflammatory reaction: A review of mechanisms and ecological implications. Ecotoxicol Environ Saf. 2021;224:112711. https://doi.org/10.1016/j.ecoenv.2021.112711.
35. Chen K, Li M, Tang Y, Lu Z. Mitochondrial reactive oxygen species initiate gasdermin D-mediated pyroptosis and contribute to paraquat-induced nephrotoxicity. Chemico-Biol Interact. 2024;390:110873. https://doi.org/10.1016/j.cbi.2024.110873.
36. Djukic MM, Jovanovic MD, Ninkovic M, Stevanovic I, Ilic K, Curcic M, et al. Protective role of glutathione reductase in paraquat induced neurotoxicity. Chemico-Biol Interact. 2012;199:74–86. https://doi.org/10.1016/j.cbi.2012.05.008.
37. Subbiah R, Tiwari RR. The herbicide paraquat-induced molecular mechanisms in the development of acute lung injury and lung fibrosis. Crit Reviews Toxicol Taylor Francis. 2021;51:36–64. https://doi.org/10.1080/10408444.2020.1864721.
38. Fussell KC, Udasin RG, Gray JP, Mishin V, Smith PJS, Heck DE, et al. Redox cycling and increased oxygen utilization contribute to diquat-induced oxidative stress and cytotoxicity in Chinese hamster ovary cells overexpressing NADPH-cytochrome P450 reductase. Free Radic Biol Med. 2011;50:874–82. https://doi.org/10.1016/j.freeradbiomed.2010.12.035.
39. Reczek CR, Birsoy K, Kong H, Martínez-Reyes I, Wang T, Gao P, et al. A CRISPR screen identifies a pathway required for paraquat-induced cell death. Nat Chem Biol Nat Publishing Group. 2017;13:1274–9. https://doi.org/10.1038/nchembio.2499.
40. Tsukamoto M, Tampo Y, Sawada M, Yonaha M. Paraquat-induced oxidative stress and dysfunction of the glutathione redox cycle in pulmonary microvascular endothelial cells. Toxicol Appl Pharmcol. 2002;178:82–92. https://doi.org/10.1006/taap.2001.9325.
41. McCarthy S, Somayajulu M, Sikorska M, Borowy-Borowski H, Pandey S. Paraquat induces oxidative stress and neuronal cell death; neuroprotection by water-soluble coenzyme Q10. Toxicol Appl Pharmcol. 2004;201:21–31. https://doi.org/10.1016/j.taap.2004.04.019.
42. Robb EL, Gawel JM, Aksentijević D, Cochemé HM, Stewart TS, Shchepinova MM, et al. Selective superoxide generation within mitochondria by the targeted redox cycler mitoparaquat. Free Radic Biol Med. 2015;89:883–94. https://doi.org/10.1016/j.freeradbiomed.2015.08.021.
43. Zhao G, Cao K, Xu C, Sun A, Lu W, Zheng Y,. Crosstalk between mitochondrial fission and oxidative stress in Paraquat-Induced apoptosis in mouse alveolar type II cells. Int J Biol Sci. 2017;13:888–900. https://doi.org/10.7150/ijbs.18468.
44. Zaidi A. Plasma membrane Ca2+-ATPases: targets of oxidative stress in brain aging and neurodegeneration. World journal of biological chemistry. Baishideng Publishing Group Inc. 2010;1:271–80. https://doi.org/10.4331/wjbc.v1.i9.271.
45. Bernardini C, Grilli E, Duvigneau JC, Zannoni A, Tugnoli B, Gentilini F, et al. Cellular stress marker alteration and inflammatory response in pigs fed with an Ochratoxin contaminated diet. Res Vet Sci. 2014;97:244–50. https://doi.org/10.1016/j.rvsc.2014.07.018.
46. Brenner C. Mitochondrial membrane permeabilization in apoptosis. In: Schwab M, editor. Encyclopedia of Cancer. Berlin, Heidelberg: Springer; 2015. p. 2870–2872. https://doi.org/10.1007/978-3-642-27841-9_3767-2.
47. Zorov DB, Juhaszova M, Sollott SJ. Mitochondrial reactive oxygen species (ROS) and ROS-induced ROS release. Physiol Rev. 2014;94:909–50. https://doi.org/10.1152/physrev.00026.2013.
48. Alak G, Özgeriş FB, Yeltekin AÇ, Parlak V, Ucar A, Caglar O, et al. Hematological and hepatic effects of ulexite in zebrafish. Environ Toxicol Pharmacol. 2020;80:103496. https://doi.org/10.1016/j.etap.2020.103496.
49. Hazman Ö, Bozkurt MF, Fidan AF, Uysal FE, Çelik S. The effect of boric acid and borax on oxidative stress, inflammation, ER stress and apoptosis in cisplatin toxication and nephrotoxicity developing as a result of toxication. Inflammation. 2018;41:1032–48. https://doi.org/10.1007/s10753-018-0756-0.
50. Ince S, Kucukkurt I, Cigerci IH, Fatih Fidan A, Eryavuz A. The effects of dietary boric acid and borax supplementation on lipid peroxidation, antioxidant activity, and DNA damage in rats. J Trace Elem Med Biol. 2010;24:161–4. https://doi.org/10.1016/j.jtemb.2010.01.003.
51. Ince S, Kucukkurt I, Demirel HH, Acaroz DA, Akbel E, Cigerci IH. Protective effects of boron on cyclophosphamide induced lipid peroxidation and genotoxicity in rats. Chemosphere. 2014;108:197–204. https://doi.org/10.1016/j.chemosphere.2014.01.038.
52. Kucukkurt I, Akbel E, Karabag F, Ince S. The effects of dietary boron compounds in supplemented diet on hormonal activity and some biochemical parameters in rats. Toxicol Ind Health. 2015;31:255–60. https://doi.org/10.1177/0748233712469648.
53. Cengiz M, Sahinturk V, Yildiz SC, Sahin IK, Namık B, et al. Cyclophosphamide induced oxidative stress, lipid per oxidation, apoptosis and histopathological changes in rats: Protective role of boron. J Trace Elem Med Biol. 2020;62:126574–126574. https://doi.org/10.1016/J.JTEMB.2020.126574.
54. Turkez H, Tozlu OO, Arslan ME, Baba C, Saracoglu MM, Yıldız E, et al. Boric acid and borax protect human lymphocytes from oxidative stress and genotoxicity induced by 3-Monochloropropane-1,2-diol. Biol Trace Elem Res. 2024;202:5006–16. https://doi.org/10.1007/s12011-024-04060-4.
55. Dong Y, Wang J, Feng D, Qin H, Wen H, Yin Z, et al. Protective effect of quercetin against oxidative stress and brain edema in an experimental rat model of subarachnoid hemorrhage. Int J Med Sci Ivyspring Int Publisher. 2014;11:282–90. https://doi.org/10.7150/ijms.7634.
56. Peng C, Li H, Mao Q, Tang K, Sun M, Ai Q, et al. Quercetin inhibits hydrogen peroxide-induced cleavage of heat shock protein 90 to prevent glutathione peroxidase 4 degradation *via* chaperone-mediated autophagy. Phytomedicine. 2025;136:156286. https://doi.org/10.1016/j.phymed.2024.156286.
57. Phachonpai W, Wattanathorn J, Muchimapura S, Tong-Un T, Preechagoon D. Neuroprotective effect of Quercetin encapsulated liposomes: A novel therapeutic strategy against alzheimer's disease. Am J Appl Sci. 2010;7:480–5. https://doi.org/10.3844/ajassp.2010.480.485.
58. de Oliveira MR, de Souza ICC, Fürstenau CR. Carnosic acid induces Anti-inflammatory effects in paraquat-treated SH-SY5Y cells through a mechanism involving a crosstalk between the Nrf2/HO-1 axis and NF-κB. Mol Neurobiol. 2018;55:890–7. https://doi.org/10.1007/s12035-017-0389-6.
59. Henkler F, Baumann B, Fotin-Mleczek M, Weingärtner M, Schwenzer R, Peters N, et al. Caspase-mediated cleavage converts the tumor necrosis factor (TNF) receptor-associated factor (TRAF)-1 from a selective modulator of TNF receptor signaling to a general inhibitor of NF-κB Activation *. J Biol Chem Elsevier. 2003;278:29216–30. https://doi.org/10.1074/jbc.M211090200.
60. Sun J, Tian T, Wang Y, Yan W, Zhang B, Wang K, et al. Paraquat-activated BV-2 microglia induces neuroinflammatory responses in the neuron model through NF-κB signaling pathway. Toxicol in Vitro. 2021;72:105076. https://doi.org/10.1016/j.tiv.2021.105076.
61. Liu T, Zheng F, Liu L, Zhou H, Shen T, Li Y, et al. Paraquat disrupts the blood–brain barrier by increasing IL-6 expression and oxidative stress through the activation of PI3K/AKT signaling pathway. Open Med. 2024;19(1):20241020. https://doi.org/10.1515/med-2024-1020.
62. Chang X, Lu W, Dou T, Wang X, Lou D, Sun X, et al. Paraquat inhibits cell viability via enhanced oxidative stress and apoptosis in human neural progenitor cells. Chemico-Biol Interact. 2013;206:248–55. https://doi.org/10.1016/j.cbi.2013.09.010.
63. Chen YW, Yang YT, Hung DZ, Su CC, Chen KL. Paraquat induces lung alveolar epithelial cell apoptosis via Nrf-2-regulated mitochondrial dysfunction and ER stress. Arch Toxicol. 2012;86:1547–58. https://doi.org/10.1007/s00204-012-0873-8.
64. Choi SE, Park YS, Koh HC. NF-κB/p53-activated inflammatory response involves in diquat-induced mitochondrial dysfunction and apoptosis. Environ Toxicol. 2018;33:1005–18. https://doi.org/10.1002/tox.22552.
65. Wang S, Zhu X, Xiong L, Ren J. Ablation of Akt2 prevents paraquat-induced myocardial mitochondrial injury and contractile dysfunction: role of Nrf2. Toxicol Lett. 2017;269:1–14. https://doi.org/10.1016/j.toxlet.2017.01.009.
66. Hu W, Wang Y, Cheng B, Xu L, Zhou Y, Wu L. Protective effect of electrical stimulation of the vagus nerve in lipopolysaccharide–induced acute lung injury in rats. Mol Med Rep. 2021;23:365. https://doi.org/10.3892/mmr.2021.12004.
67. Kahraman E, Göker E. Boric acid exert anti-cancer effect in poorly differentiated hepatocellular carcinoma cells via inhibition of AKT signaling pathway. J Trace Elem Med Biol. 2022;73:127043. https://doi.org/10.1016/j.jtemb.2022.127043.
68. Ahmadian E, Eftekhari A, Kavetskyy T, Khosroushahi AY, Turksoy VA, Khalilov R. Effects of Quercetin loaded nanostructured lipid carriers on the paraquat-induced toxicity in human lymphocytes. Pestic Biochem Physiol. 2020;167:104586. https://doi.org/10.1016/j.pestbp.2020.104586.

69. Tepedelen BE, Soya E, Korkmaz M. Boric acid reduces the formation of DNA double strand breaks and accelerates wound healing process. Biol Trace Elem Res. 2016;174:309–18. https://doi.org/10.1007/s12011-016-0729-9.
70. Park C, So HS, Shin CH, Baek SH, Moon BS, Shin SH, et al. Quercetin protects the hydrogen peroxide-induced apoptosis via Inhibition of mitochondrial dysfunction in H9c2 cardiomyoblast cells. Biochem Pharmacol. 2003;66:1287–95.
71. Shahzad S, Batool Z, Afzal A, Haider S. Reversal of oxidative stress, cytokine toxicity and DNA fragmentation by quercetin in dizocilpine-induced animal model of schizophrenia. Metab Brain Dis. 2022;37:2793–805. https://doi.org/10.1007/s11011-022-01090-6.
72. Kishore AS, Surekha PA, Sekhar PVR, Srinivas A, Murthy PB. Hen egg chorioallantoic membrane bioassay: an in vitro alternative to draize eye irritation test for pesticide screening. Int J Toxicol SAGE Publications Inc. 2008;27:449–53. https://doi.org/10.1080/10915810802656996.
73. Colle D, Farina M. Oxidative stress in paraquat-induced damage to nervous tissues. In: Patel VB, Preedy VR, editors. Toxicology. Academic Press; 2021. p. 69–78. https://doi.org/10.1016/B978-0-12-819092-0.00008-X.
74. Chapouly C, Tadesse Argaw A, Horng S, Castro K, Zhang J, Asp L, et al. Astrocytic TYMP and VEGFA drive blood–brain barrier opening in inflammatory central nervous system lesions. Brain. 2015;138:1548–67. https://doi.org/10.1093/brain/awv077.

Publisher's note

Springer Nature remains neutral with regard to jurisdictional claims in published maps and institutional affiliations.